Structural, Dielectric, and Magnetic Studies of ZnCuFe2O4 Nanoparticles

Baba Basha D (dbababasha@gmail.com)
Majmaah University

Research Article

Keywords: Ferrites, Nanoparticles, X-ray diffraction, Morphology, Dielectric constant

Posted Date: May 25th, 2021

DOI: https://doi.org/10.21203/rs.3.rs-547019/v1

Abstract

The zinc copper ferrite nanoparticles were synthesized via hydrothermal method. Further, the X-ray diffraction patterns confirmed the formation of cubic spinel structure. The microstructure was analyzed using the FESEM and TEM study. The results revealed that the symmetrical and asymmetrical nanospheres were found in the surface morphology. The dielectric studies indicated that the behavior of dielectric constant and dielectric loss as a function of frequency and composition. In addition, the Maxwell-Wagner interfacial polarization was observed. Similarly, the ac-electrical conductivity behavior was well understood. The M-H loops indicated the ferromagnetic behavior of ZnCu ferrite samples.

1. Introduction

Ferrites were normally the magnetic spinel structures with a chemical formula of AFe_2O_4 (where 'A' corresponds to divalent cations like Ni, Mg, Zn, Co, Cu, Mn, etc.,). It was also known fact that the ferrite in nanoform showed various applications in science and technological field. These applications were obtained due to the predominant electrical, magnetic, electromagnetic, chemical, microwave, photocatalytic properties etc., [1]. Among all the ferrites, $NiFe_2O_4$, $MgFe_2O_4$, $ZnFe_2O_4$, $CuFe_2O_4$, $MnFe_2O_4$, etc., [1] were extensively studied for various electrical and magnetic properties.

In general, the inverse spinel ferrites showed much attention owing to their extraordinary magneto-crystalline energy, magnetization, and magnetic structure [1]. Among the above-mentioned ferrites, zinc ferrites were found to be inverse spinel, wherein, the zinc cations occupy the tetrahedral (A) site while the ferric ions occupy the tetrahedral (A) and octahedral (B) equally [2]. In nanoform, these were investigated for electrical, magnetic, and photocatalytic properties [3]. In addition, the band gap of 1.9 eV was noticed for zinc ferrite samples [4]. As a result, zinc ferrites offered applications like drug delivery, magnetic hyperthermia, sensors, photocatalytic, magnetic resonance imaging (MRI), and antimicrobial activity [5]. Several synthesis methods like sol-gel combustion, conventional heating, microwave heating, microwave assisted combustion, modified sol-gel, hydrothermal, green synthesis, combustion synthesis, and microwave assisted green synthesis were used to prepare the bulk, and nano zinc ferrites [6, 7].

Similarly, the copper ferrites were known to be ferromagnetic materials exhibiting the cubic and tetragonal structures [8]. Due to Jahn-Teller distortion, the structural phase transition (SPT) was observed in case of copper ferrites [8]. In the literature, the copper ferrites were prepared using the mechanochemical reactions, co-precipitation, sol-gel auto-combustion, and hydrothermal methods were used to prepare the copper ferrites [9]. Previous scientists clearly indicated the effect of pH on magnetic behavior of nano copper ferrites [10]. These results also showed the similar pH effect on the formation of single-phase structure. From the wide literature survey, it was confirmed that the research work on the zinc and copper ferrites was done elaborately. At this moment, the present work is well focused on doping of copper cations into the zinc ferrite spinel structures. Therefore, this work can become novel and studying the effect of copper cations on inverse spinel (zinc ferrite) system and its properties like structure, magnetic, and dielectric properties. Thus, a series of $Cu_{1-x}Zn_xFe_2O_4$ (x = 0.02, 0.04, 0.06 & 0.08)

nanoparticles were prepared using the low temperature hydrothermal techniques followed by several characterizations such as X-ray diffraction patterns, microstructure, ac-conductivity, and room temperature dielectric properties.

2. Materials, And Methods

For the preparation of ZnCu ferrite nanoparticles, the starting materials were chosen as $Zn(NO_3)_2 .6H_2O$ (99.8 % purity, Sigma-Aldrich), $Fe(NO_3)_3.9H_2O$ (99.8 % purity, Sigma-Aldrich), $Cu(NO_3)_2$ (99.8 % purity, Sigma-Aldrich), and NaOH pellets. These materials in a stoichiometric ratio were dissolved in distilled water and stirred for half an hour with a stirring rate of 450 rpm. The mixed solution was transferred to a Teflon bowl of 300 ml. Later, it was kept in a stainless-steel autoclave. This autoclave was kept in hot air oven and the hydrothermal reaction was carried out at a temperature of 150^oC/6 hr. Once the reaction is over, the oven was cooled to room temperature. Immediately, the autoclave was removed from oven and further, the Teflon bowl was kept out. The remained solution under the depth of Teflon bowl was centrifuged. Then, the nanopowder was dried at 60^oC for 2 hours. In the next step, the nano ferrites were subjected to various analysis works like X-ray diffractometer (XRD, Bruker, $Cu_{K\alpha}$, $\lambda = 0.15406$ nm), transmission electron microscope (TEM: Model Tecnai G20, FEI, USA), field-emission scanning electron microscope (FE-SEM, Ultra 55, Carl Zeiss), vibrating sample magnetometer (VSM), and LCR controller (HIOKI 3532-50, 42 Hz–8 MHz) to study the structural, morphological, and dielectric properties, respectively.

3. Results And Discussion

The X-ray diffraction (XRD) patterns of copper zinc ferrites were shown in Fig. 1. It was clear from XRD patterns that the x = 0.02–0.08 samples revealed the single-phase cubic spinel structure. Thus, it was confirmed that there were no impurity peaks in the diffraction patterns. Hence, the prepared samples were found to be high pure in nature. Moreover, the high crystallinity was noticed for all the crystalline planes. The maximum intensity was noticed for (3110 reflection plane. Further, the average crystallite size (D) was determined using the Scherrer equation [11]. The results showed that the ‘D’ value was increased from 19 to 36 nm as a function of ‘x’. This confirmed a fact that the crystallite size was increased with zinc content. This behavior was attributed to the decreasing trend of full width half maxima (FWHM, β) from 0.042 to 0.017 radian as a function of ‘x’. This established a fact that there exists an inversely proportional relation between the crystallite size, and FWHM. The similar observations were found in the literature [10]. Besides, the lattice parameters were determined, and the results showed that the lattice constants were found to be increasing from 8.341 to 8.371 Å with increase of zinc content in the copper ferrite system. This kind of trend was occurred due to the increase of compositional molecular weight (C.M.W) from 182.08 to 182.191 g/mole. Moreover, the ionic radius zinc cation (0.60 Å) is greater than the copper cation (0.57 Å). This clearly showed that the incorporation of zinc cations usually increases the unit cell volume followed by increasing the lattice constants. Thus, unit cell volume was also increased with composition. In addition, the X-ray density (ρ_x) was decreased from 4.171 to 4.125 g/cm^3

as a function of ‘x’. Finally, the specific surface area (S) was calculated, and the results were observed to be decreasing from 131.6 to 68.8 m^2/g with ‘x’. The surface morphology of ZnCu ferrites was analyzed using the field emission scanning (FESEM), and transmission electron microscopy (TEM) pictures. It was found that the x = 0.02–0.08 compositions showed the presence of bigger grains, and smaller sized grains. Especially, the x = 0.02 sample showed asymmetrical, and bigger sized grains. On the other hand, the x = 0.04–0.08 samples revealed the small sized grains. Besides, the grains were in close contact with the other grains. This kind of behavior was attributed to the agglomeration effect []. Further, the TEM pictures revealed the asymmetrical spheres like nanoparticles. These nanoparticles were also very close to each other due to agglomeration [10]. It was also confirmed that the surface morphology of samples using FESEM, and TEM was in close agreement with each other. Moreover, these results established a fact that the formation of ZnCu ferrite nanoparticles was confirmed from microstructure.

Table.1 XRD parameters of ZnCu ferrites.

x	0.02	0.04	0.06	0.08
D_a (nm)	19	24	28	36
FWHM (radian)	0.042	0.032	0.025	0.017
a = b = c (Å)	8.341	8.358	8.369	8.371
Max. intense plane	(311)	(311)	(311)	(311)
V $(Å)^3$	580.30	583.85	586.16	586.58
C.M.W (g/mole)	182.08	182.118	182,155	182.191
ρ_x (g/c.c.)	4.171	4.142	4.131	4.125
S (m^2/g)	131.6	103.5	88.4	68.8

The dielectric property is an important aspect to explain the behavior of microstructural species such as grain, grain boundaries. For this, the frequency dependence of dielectric constant (ε'), and dielectric loss (ε") plots were drawn as shown in Fig. 2. The dielectric constant versus frequency plots of ZnCu ferrites indicated that the dielectric constant was noticed to be high at low input field frequencies. On the other hand, the similar parameter was decreased to very small values at high input field frequencies. This was noticed to be a usual dielectric behavior. That is, obtaining the high, and low dielectric constant values at low, and high frequencies, respectively. Likewise, the dielectric loss parameter obtained for all zinc copper ferrite nanoparticles showed the same trend. This kind of nature was achieved due to the Maxwell-Wagner’s interfacial polarization, and inhomogeneous dielectric structure [11, 12–15]. Moreover, the microstructural species could be responsible for the same behavior. That is, the grain boundaries play a vital role achieving the high dielectric behavior at low frequencies, while the grains fulfill the rest of the role to receive the low dielectric behavior at high frequencies. Usually, the charge carriers will be piled up the grain boundary interface at low electric field frequencies. At this moment, the energy of the carriers

will be very less than the energy of the grain boundary. Hence, the carriers cannot penetrate through the grain boundary. This leads to the piling up of carriers at the interface. However, the increasing value of the input frequency reinforces the energy of charge carriers. Hence, the carriers can break the grain boundary, and therefore, they pass through the grain boundary. This leads to the decrease of grain boundary resistance. Further, they enter the grain segment. As a result, the low resistivity will be developed leading to high conductivity. It can be understood that the high resistive grain boundaries are predominant at low frequencies, whereas the low resistive grains are active at high frequencies. Later, the dielectric modulus properties like $M' = \varepsilon'/(\varepsilon'^2+\varepsilon''^2)$ (real part), and $M'' = \varepsilon''/(\varepsilon'^2+\varepsilon''^2)$ (imaginary part) were calculated [16]. The corresponding plots such as M' - log ω, and M" - log ω were shown in Fig. 3. These plots revealed that the M', and M" showed zero values at low frequencies. It was attributed to the mobility of charge carriers for the longer distances, and thus, they cannot have the ability to control their mobility. Hence, restoring force will be diminished [17]. On the other hand, the increase of input frequency allowed increasing the M', and M" values. Moreover, at high frequencies, the relaxations were found. In particular, the M" versus frequency plots of ZnCu ferrites, provided the relaxation frequencies varying from log ω = 5.426 to 5.734. It was also found that the variation of relaxation frequencies was not systematic as a function of composition. This was attributed to the mobility of mobile charges within the samples. The long-range and short-range polarization regions were observed in the M"-log ω plots on either side of relaxation portions such as below, and above the relaxation regions, respectively [18–20]. The magnetic behavior of the ZnCu ferrite samples was well understood using the magnetization versus magnetic field (M-H) curves as depicted in Fig. 4. The M-H loops showed that the x = 0.02–0.08 samples showed the maximum magnetization varying from 4.5 to 2.7 emu/g. It was also seen that the all the plots were not of completely saturation. This can be attributed to the cation distribution between the tetrahedral (A), and octahedral (B) sites. Similarly, the coercivity was noted to be changing from 516 to 148 Oe (inset Fig. 4), while the retentivity was altered from 1.248 to 0.681 emu/g. These plots indicated a fact that all the ferrite samples showed the soft ferrite nature due to low coercivity, and further, these samples can be suitable for soft magnet manufacturing device applications [10].

4. Conclusions

The $Cu_{1-x}Zn_xFe_2O_4$ (x = 0.02, 0.04, 0.06 & 0.08) nanoparticles were synthesized via hydrothermal technique. The XRD showed the single-phase cubic spinel structure. The lattice constants were found to be increasing from 8.341 to 8.371 Å with increase of zinc content in the copper ferrite system. This confirmed the expansion of unit cell in case of ZnCu ferrites. In addition, the spherical grains, and nanoparticles were seen in FESEM, and TEM pictures. Further, dielectric properties clearly showed the space charge polarization mechanism at lower frequencies. Moreover, the M-H loops revealed the ferromagnetic nature of ZnCu ferrites.

Declarations

Conflicts of Interest: Authors declare no conflicts of interest.

Acknowledgements: The author would like to thank Deanship of Scientific Research at Majmaah University for supporting this work under Project Number No……..

References

1. K.C. Babu Naidu, W. Madhuri, Hydrothermal synthesis of $NiFe_2O_4$ nano-particles: structural, morphological, optical, electrical and magnetic properties. Bull. Mater. Sci. **40**, 417–425 (2017). https://doi.org/10.1007/s12034-017-1374-4
2. T.V. Sagar, T.S. Rao, K.C. Babu Naidu (2020). AC-electrical conductivity, magnetic susceptibility, dielectric modulus, and impedance studies of Sol-Gel processed nano-NiMgZn ferrites. Mater. Chem. Phys., 123902. doi:10.1016/j.matchemphys.2020.123902
3. M. Madhukara Naik, B. Naik, H.S. Nagaraju, G. Vinuth, M.Raja Naika, H., & K. Vinu, Green synthesis of zinc ferrite nanoparticles in Limonia acidissima juice: Characterization and their application as photocatalytic and antibacterial activities. Microchem. J. (2019). doi:10.1016/j.microc.2019.02.059
4. S.M. Hoque, M.S. Hossain, S. Choudhury, S. Akhter, F. Hyder, Synthesis and characterization of $ZnFe_2O_4$ nanoparticles and its biomedical applications. Mater. Lett. **162**, 60–63 (2016). doi:10.1016/j.matlet.2015.09.066
5. M.G. Naseri, E.B. Saion, M. Hashim, A.H. Shaari, H.A. Ahangar, Synthesis and characterization of zinc ferrite nanoparticles by a thermal treatment method. Solid State Commun. **151**(14–15), 1031–1035 (2011). doi:10.1016/j.ssc.2011.04.018
6. Y. Ding, Y. Yang, H. Shao, High capacity $ZnFe_2O_4$ anode material for lithium ion batteries. Electrochim. Acta **56**(25), 9433–9438 (2011). doi:10.1016/j.electacta.2011.08.031
7. A. Tony Dhiwahar, M. Sundararajan, P. Sakthivel, C.S. Dash, S. Yuvaraj (2019). Microwave-assisted combustion synthesis of pure and zinc-doped copper ferrite nanoparticles: Structural, morphological, optical, vibrational, and magnetic behavior. J. Phys. Chem. Solids, 109257. doi:10.1016/j.jpcs.2019.109257
8. R. Köferstein, T. Walther, D. Hesse, S.G. Ebbinghaus, Crystallite-growth, phase transition, magnetic properties, and sintering behaviour of nano-CuFe2O4 powders prepared by a combustion-like process. J. Solid State Chem. **213**, 57–64 (2014). doi:10.1016/j.jssc.2014.02.010
9. K. Kombaiah, J.J. Vijaya, L.J. Kennedy, M. Bououdina, Optical, magnetic and structural properties of $ZnFe_2O_4$ nanoparticles synthesized by conventional and microwave assisted combustion method: A comparative investigation. Optik - International Journal for Light and Electron Optics **129**, 57–68 (2017). doi:10.1016/j.ijleo.2016.10.058
10. T. Ramaprasad, R.J. Kumar, U. Naresh, M. Prakash, D. Kothandan, K.C.B. Naidu, Effect of pH value on structural and magnetic properties of $CuFe_2O_4$ nanoparticles synthesized by low temperature hydrothermal technique, Mater. Res. Express, 5 (2018), p. 095025, 10.1088/2053 – 1591/aad860
11. P. Scherrer, Bestimmung der Grosse und der Inneren Struktur von Kolloidteilchen Mittels Rontgenstrahlen, Nachrichten von der Gesellschaft der Wissenschaften, Gottingen. Mathematisch-

Physikalische Klasse **2**, 98–100 (1918)

12. K.W. Wagner, The Distribution of Relaxation Times in Typical Dielectrics. Ann. Phys. **40**, 817 (1913)
13. Q. Hou, K. Sun, P. Xie, K. Yan, R.F.Y. Liu, Ultrahigh dielectric loss of epsilon-negative copper granular composites. Mater. Lett. **169**, 86–89 (2016). http://dx.doi.org/10.1016/j.matlet.2016.01.092
14. D. Baba Basha, An improved dielectric behavior of hydrothermally synthesized $Ba_{0.4}La_{0.6-y}Eu_yTiO_3$ (y = 0.01–0.04) nanorods. J. Mater. Sci.: Mater. Electron. (2021). https://doi.org/10.1007/s10854-021-05297-8
15. D. Baba Basha Hydrothermal synthesis of $Ba_{1-x}La_xTiO_3$ (x = 0.2, 0.4, 0.6, & 0.8) nanorods: structure, morphology, optical band gap, and dielectricity behavior. J Mater Sci: Mater Electron 31, 16448–16458 (2020). https://doi.org/10.1007/s10854-020-04199-5
16. A. Mallikarjuna, S. Ramesh, N.S. Kumar, K. Chandra Babu Naidu, K.V. Ratnam, H. Manjunatha, B.P. Rao, Structural transformation and high negative dielectric constant behaviour in (1-x) $(Al_{0.2}La_{0.8}TiO_3)$ + (x) $(BiFeO_3)$ (x = 0.2–0.8) nanocomposites. Physica E **122**, 114204 (2020)
17. A. Mallikarjuna, S. Ramesh, N. Suresh Kumar, K. Chandra Babu Naidu, K. Venkata Ratnam, H. Manjunatha, Photocatalytic activity, negative ac- electrical conductivity, dielectric modulus, and impedance properties in 0.6 $(Al_{0.2}La_{0.8}TiO_3)$ + 0.4 $(BiFeO_3)$ nanocomposite. Cryst. Res. Technol. **55**, 1–10 (2020) 202000068
18. N. Suresh Kumar, R. Padma Suvarna, K. Chandra Babu Naidu, Negative dielectric behavior in tetragonal $La_{0.8}Co_{0.2-x}Eu_xTiO_3$ (x = 0.01–0.04) nanorods. Mater. Charact. **166**, 110425 (2020)
19. S. Dastagiri, M.V. Lakshmaiah, K. Chandra Babu Naidu, N. Suresh Kumar, A. Khan, Induced dielectric behavior in high dense $Al_xLa_{1-x}TiO_3$ (x = 0.2–0.8) Nanospheres. J. Mater. Sci.: Mater. Electron. **30**, 20253–20264 (2019)
20. N. Suresh Kumar, R. Padma Suvarna, K.C.B. Naidu, G. Ranjith Kumar, S. Ramesh, Structural and Functional Properties of Sol-Gel Synthesized and Microwave Heated $Pb_{0.8}Co_{0.2-z}La_zTiO_3$ (z = 0.05–0.2) Nanoparticles. Ceram. Int. **44**, 19408–19420 (2018)
21. N.S. Kumar, R.P. Suvarna, K.C.B. Naidu, Sol-Gel Synthesized and Microwave Heated $Pb_{0.8-y}La_yCo_{0.2}TiO_3$ (y = 0.2–0.8) Nanoparticles: Structural, Morphological and Dielectric Properties. Ceram. Int. **44**, 18189–18199 (2018)

Figures

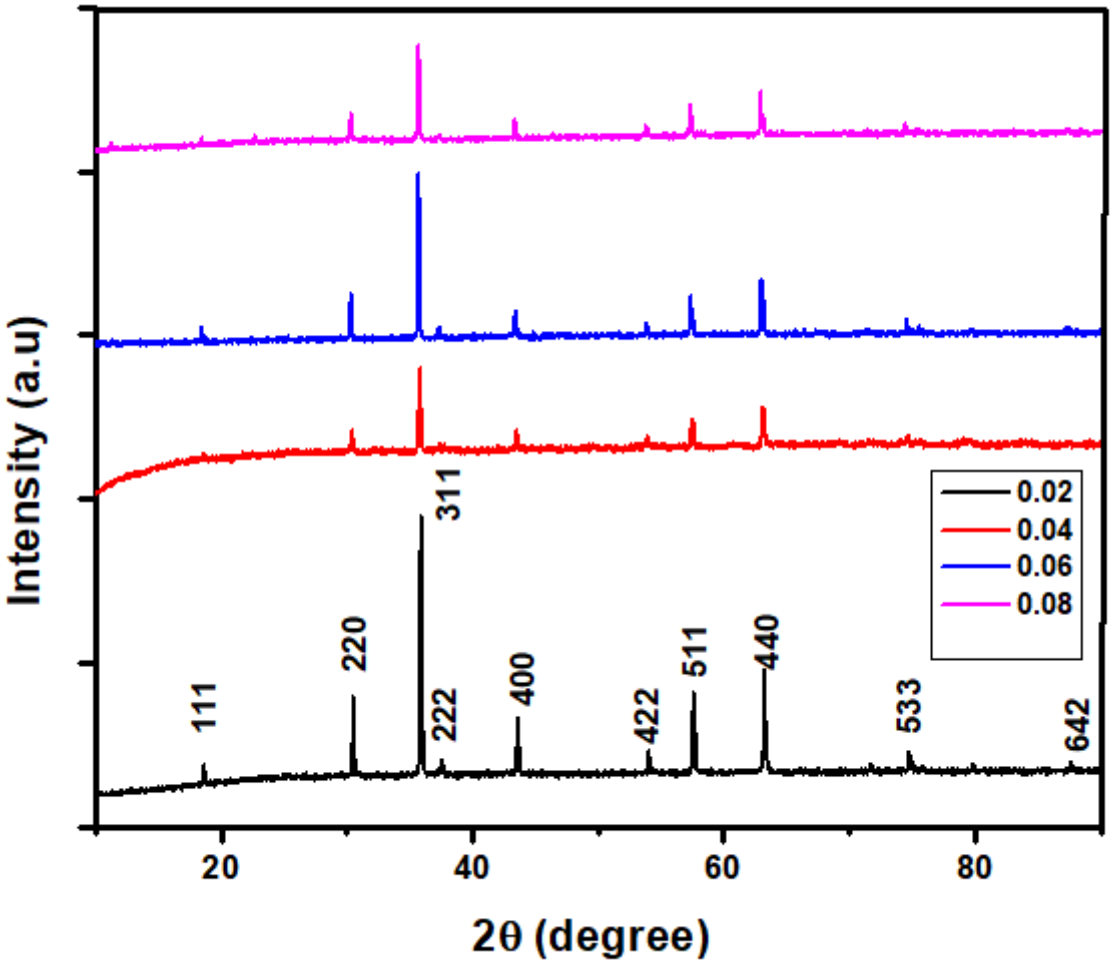

Figure 1

XRD patterns of ZnCu ferrites

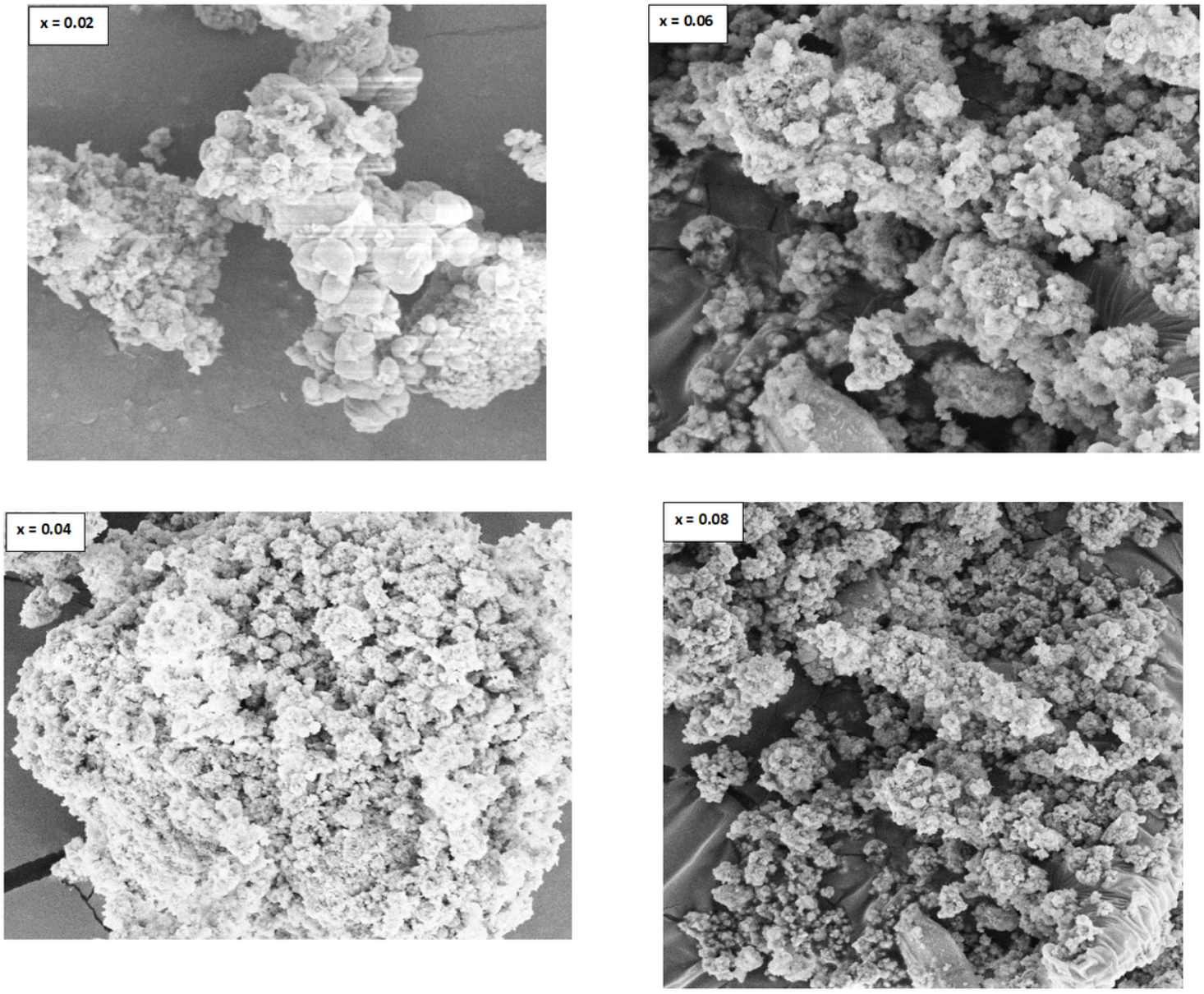

Figure 2

FESEM pictures of ZnCu ferrites

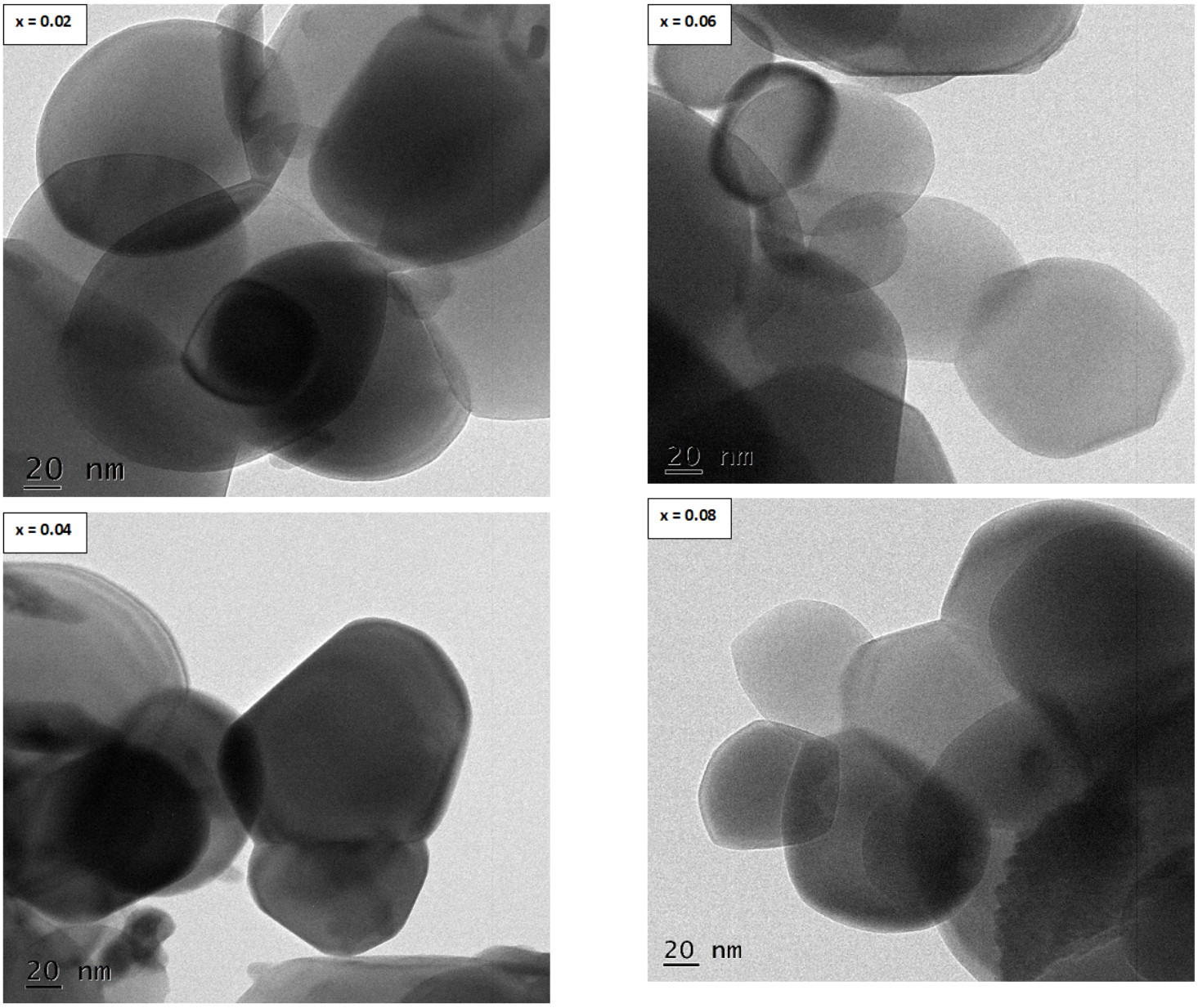

Figure 3

TEM pictures of ZnCu ferrites

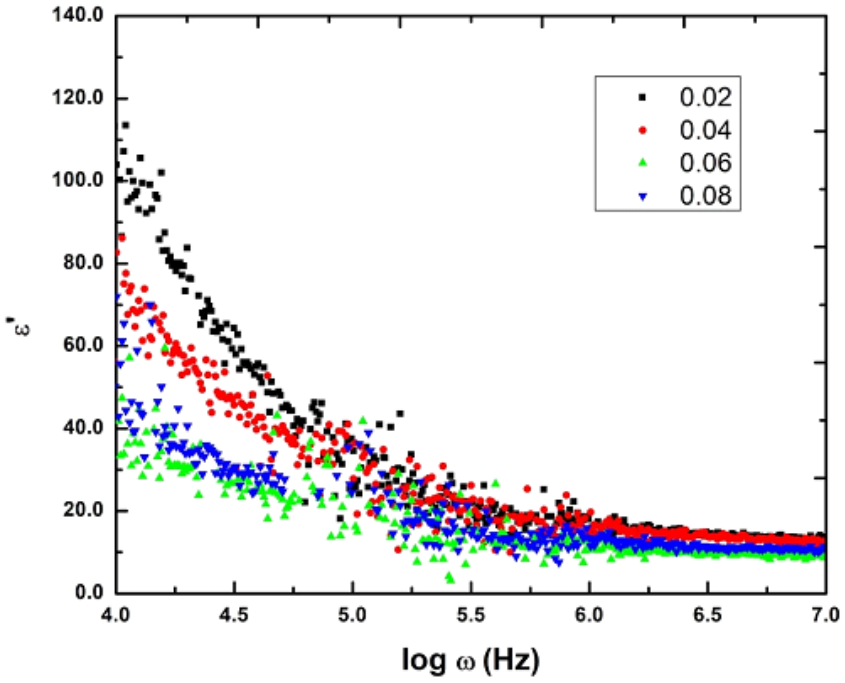

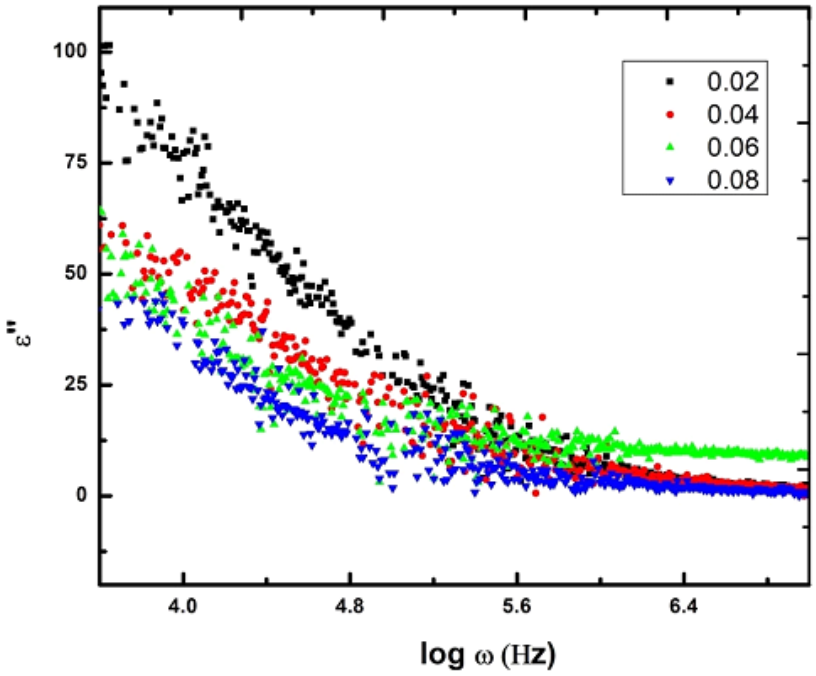

Figure 4

Frequency dependence of dielectric constant (ε'), and dielectric loss (ε'')

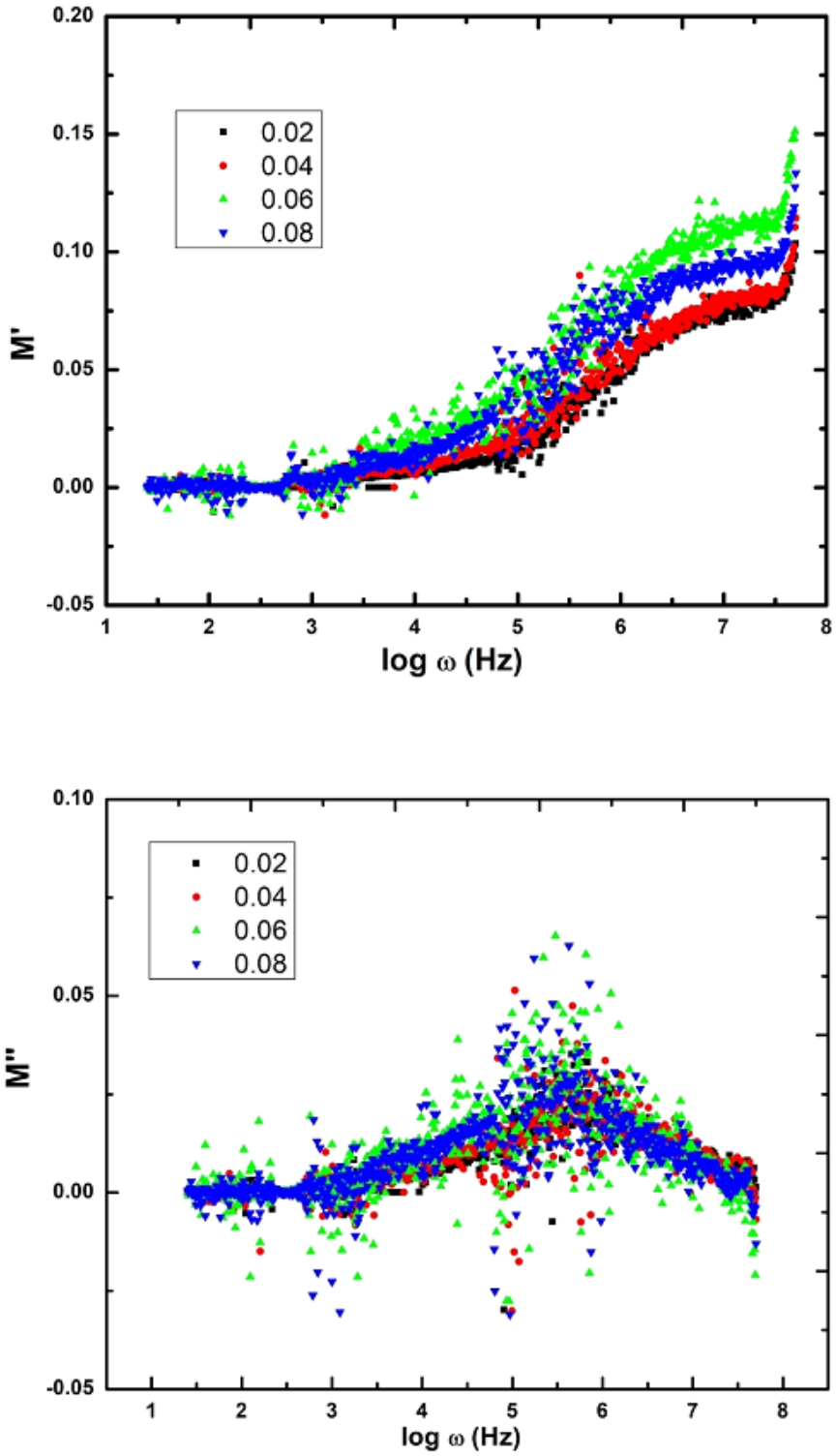

Figure 5

Frequency dependence of M', and M"

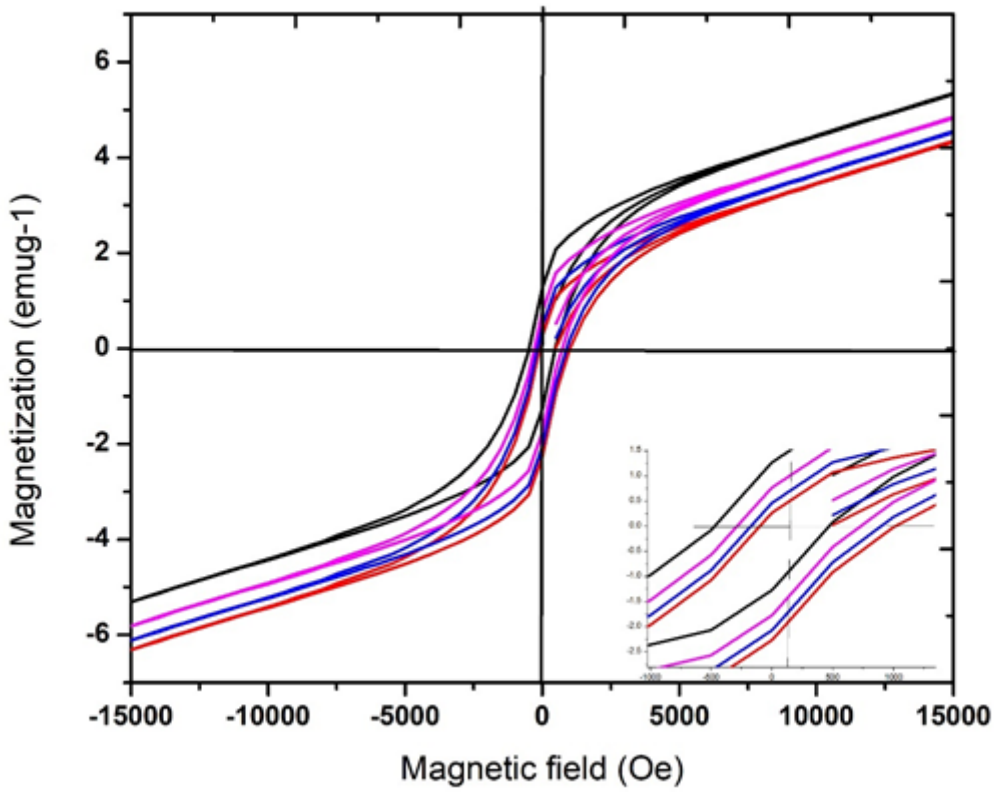

Figure 6

M-H loops of ZnCu ferrites